ResearchGate

See discussions, stats, and author profiles for this publication at: https://www.researchgate.net/publication/232927778

A Blind Comparison Between Results of Four Image Analysis Systems Using a Photo-Library of Piles of Sieved Fragments

Article *in* Fragblast · August 2010

DOI: 10.1076/frag.7.2.105.15899

CITATIONS
48

READS
573

6 authors, including:

John-Paul Latham
Imperial College London
160 PUBLICATIONS **4,179** CITATIONS

SEE PROFILE

Maerz Norbert
Missouri University of Science and Technology
103 PUBLICATIONS **2,171** CITATIONS

SEE PROFILE

Michael Noy
10 PUBLICATIONS **91** CITATIONS

SEE PROFILE

Simon Tose
AEL Mining Services
2 PUBLICATIONS **49** CITATIONS

SEE PROFILE

All content following this page was uploaded by Simon Tose on 02 May 2018.

The user has requested enhancement of the downloaded file.

Fragblast
2003, Vol. 7, No. 2, pp. 105–132

1385-514x/03/0702-105$16.00
© Swets & Zeitlinger

A Blind Comparison Between Results of Four Image Analysis Systems Using a Photo-Library of Piles of Sieved Fragments

JOHN-PAUL LATHAM[1], JOHN KEMENY[2], NORBERT MAERZ[3], MICHAEL NOY[4], JACQUES SCHLEIFER[5] AND SIMON TOSE[6]

ABSTRACT

Four image analysis systems for measuring rock fragmentation: FragScan, PowerSieve®, Split and WipFrag, have been compared under conditions necessary to provide an objective though limited assessment of their capabilities. The analysis of results is based on a sample of ten photographs taken from a series of photographs of controlled artificial muckpiles. These were created from dumping a blended mixture of sieved samples of limestone aggregate, in order to create a range of near perfect Rosin–Rammler sieve size distributions. Results from the various systems are compared with sieved results using both histogram and cumulative forms, with and without fines corrections in the case of Split and Wipfrag. Statistical indicators are evaluated to examine the match between system prediction values and sieving values. Commentaries on the results by the inventors of each system have been incorporated. All four systems were found to perform both well in some cases and poorly in others. From a detailed examination of the results, some insight into the strengths and weaknesses of the various systems is presented.

Keywords: Image analysis, size distribution, fragmentation, sampling bias.

1. INTRODUCTION

1.1. Industrial Context

Industrial applications of auto-sizing systems are numerous and while the specific systems referred to in this paper were developed in the context of mining and blast

Address correspondence to: John-Paul Latham[1], Department of Earth Science and Engineering, Imperial College, London SW7 2BP, UK. Tel.: +44 (0)20 7594 7327; E-mail: j.p.latham@ic.ac.uk
[2]Department of Mining and Geological Engineering, University of Arizona, Tucson, AZ, USA. Tel.: +1 520 621 4448; E-mail: kemeny@u.arizona.edu
[3]Rock Mechanics and Explosives Research Centre, University of Missouri-Rolla, MO, USA. Tel.: +1 573 341 4317; E-mail: norbert@umr.edu
[4]Orica Australia Pty Ltd., Australia. Tel.: +612 4939 5200; E-mail: michael.noy@orica.com
[5]Ecole des Mines de Paris, Paris, France. Tel.: +33 1 64 69 48 88; E-mail: schleiff@cges.ensmp.fr
[6]Blast Consult, African Explosives Ltd., South Africa. Tel.: +27 11 606 2116; E-mail: toses@ael.co.za

fragmentation assessment, they are finding widespread use in other industrial fields of materials processing. Automated measurement of blast fragmentation has gone through two decades of rapid development and is now a generally accepted tool in the mining and mineral processing industries. An extensive source of literature on the subject can be found. For example, a seminal monograph on measurement of blast fragmentation was presented as the proceedings of the Fragblast-5 workshop [1]. The keynote paper at this workshop given by Cunningham [2] provides an excellent introduction to the motivation for such systems and the many potential pitfalls arising from their use. Researchers aiming to improve models of fragmentation blasting have long awaited the technology to provide a means of comparing the predicted fragmentation of a blast with the actual fragmentation found in the blastpile. The link between more accurate and rapid fragmentation assessment and more optimal blast design, via the use of better empirical and numerical models, is widely recognized. It was therefore of interest to take a snap-shot (in August 1999) of the capability of several available systems designed to predict sieve size distributions from photographic or video image data. Reference to the underlying principles behind each different system is necessarily kept to a minimum as these can be found in the literature.

1.2. Background to the Comparison Study

An opportunity was presented in Johannesburg at the Fragblast-6 Symposium in August 1999, where representatives of four automated size analysis systems offered to perform blind assessments on a subset of ten library photographs. Each high quality photograph presented a different artificially produced laboratory blastpile of known sieve size distribution. Analysis results were processed rapidly and given in terms of best-fit Rosin–Rammler coefficients. With the exception of FragScan operators, the Rosin–Rammler coefficients for the actual sieve analysis and the imaging systems were shared while at the Symposium. Although the FragScan analysis was carried out a month later, the integrity of the blind trial was maintained. The purpose of this paper is to provide an objective set of results from which to compare certain aspects of the commercial packages: FragScan, PowerSieve®, Split and WipFrag. Results presented in this paper for each different system refer to the standard operating systems as available in August 1999 and their deployment was as described in Section 3 below. A comparison using only one photograph per size distribution is all that was available. Clearly, this is far from ideal but it provides an interesting study nonetheless. In hindsight, it would have been preferable to have created a photo-library with, say, five separate photos (for five independent surface expressions of the dumped material) per size distribution.

It is suggested, see below, that errors associated with sampling are likely to be only minor in this comparison study, partly because it is based on supplied photographs for

which data acquisition differences have been removed between the four systems. The main differences in results between the four systems can then be attributed to differences in system fidelity for the delineation of particles, differences in allocating particles to size ranges, and differences in the treatment of fines. One of the most likely causes of significant differences between the systems concerns the method of assessment of the proportion of fine material i.e., particles that cannot be resolved from images taken at a typical preset scale (e.g., a resolution setting which in normal circumstances, would be designed to concentrate on accurate quantification of the expected mean sizes). The improvements that any system can bring about by judicious use of zoom-merge sampling (e.g., [3]) are outside the scope of this paper.

The PowerSieve® and FragScan systems do not incorporate edge detection algorithms. Their ability to define appropriately the total areas and sizes of fine material below resolution within the image is considered by their inventors to arise automatically from the erosion-dilation and sizing algorithms applied and thus they do not incorporate fines corrections (as of August 1999). Split and WipFrag use edge detection algorithms. Split recognises that consideration of the 'black' areas (i.e., areas that the program does not delineate as particles in the photograph) provide a potential means of correcting the particle size analysis to help account more accurately for the fines content [4]. Similarly, WipFrag, which overlays an edge net of particle outlines (of one pixel width), recognises that its basic algorithms introduce systematic errors as the range of particle sizes is increased. Therefore, an automatic correction for fines based on the calibration of experiments on dumped rock [5] has been made available.

A previous field study to compare WipFrag, Split and FragScan systems with sieve results was reported by Liu and Tran [6]. Tests reported at that time suggested that Split and WipFrag yielded results that gave the 50% sieve size to be about 1.5 times their true sieve values while FragScan yielded results two times their true values. Since then, there have been changes in the various algorithms within the different operating systems and this paper reports the findings of a more recent comparison study.

The results are presented in full and it is hoped that they will speak for themselves. The results are presented firstly to deal with general observations based on 'routine' employment of the four systems and therefore a 'fines correction' in the case of Split and WipFrag is included. A more detailed analysis presented later in the paper includes size distribution curves and histograms showing the size analysis before and after fines corrections. Discussion points raised by authors and inventors from each of the systems are included in sections presented before the results. The photo-library is based on exact Rosin–Rammler sieve size distribution coefficients and comparison of these coefficients forms the basis of the general observations in this paper.

1.3. Size Distribution Coefficients

The most popular equations used to analyse the particle size distribution (PSD) in mineral engineering are the Rosin–Rammler equation [7] of Weibull form, Equations (1) and (2), and the Schuhmann [8] equation of power law form, Equation (3). In mineral processing and mining engineering, image analysis systems have recently focused on the development of a 'fines correction' because in certain systems, it is recognized that automated size analysis will not resolve accurate information for size ranges below the nominal camera magnification setting, even though these 'fines' may make up a significant mass proportion of the fragmented pieces. Whereas Maerz and Zhou [5] report on a fines correction factor incorporated in WipFrag, which assumes a Rosin–Rammler form to the PSD, Kemeny et al. [4] reports on a different fines correction approach adopted in Split which is based on extrapolation of the Schuhmann curve. PowerSieve® and FragScan do not incorporate a fines correction.

In Equation (1), n is the Rosin–Rammler uniformity coefficient and S_c is the Rosin–Rammler characteristic size, taken to be the 63.2 per cent passing size and y is the fraction by weight finer than a given sieve size.

$$y = 1 - \exp\left\{ -\left(\frac{S}{S_c}\right)^n \right\} \tag{1}$$

Alternatively, it may be expressed with respect to the 50% passing size S_{50} as

$$y = 1 - \exp\left\{ -0.693\left(\frac{S}{S_{50}}\right)^n \right\} \tag{2}$$

Equation (3), the Schuhmann equation, defines the family of power law curves, s is the sieve size and S_{100} represents the 100 percent passing (i.e., the maximum) sieve size while m governs the uniformity or spread of sizes.

$$y = \left(\frac{S}{S_{100}}\right)^m \tag{3}$$

When a law yielding S_{50} and n is a satisfactory fit to a given sample, then for the same S_{50}, the best power law fit may be estimated using the relation $m = 0.645n$ [9].

1.4. Photo-Library Background

The experiment leading to the production of a photo-library was carried out in the following steps [10]:

1. Approximately 100 kg of crushed limestone aggregate with sizes of less than 150 mm was collected. Coarse sand fractions were also obtained.
2. The aggregates were screened onto 12 fractions using sieves from 1 mm to 125 mm. Each aggregate fraction was weighed and its median sieve size was calculated (except for the first and last fractions).

3. A range of pre-set values of S_c and n were chosen to cover a wide range of prototype distributions. The required fractions of each size range were calculated for a specified (S_c, n) artificial blastpile. Each fraction was prepared, weighed out, mixed together and dumped into a flat rectangular pan 71.5 by 41.5 cm, giving the required artificial blastpile (S_c, n), with a typical total mass of between 30 and 40 kg.
4. A photograph was taken perpendicular to the surface of the pile. The scale bar intervals marked on the tray indicate 100 mm.

The photographs were taken under ideal laboratory conditions, but with higher contrasts and shadows than is generally preferred for automated image analysis, because their original purpose was to aid manual scanline mapping of particle boundaries. The dumping action attempted to minimise vibration of the tray and mimic the surface appearance of an unsegregated mixture. The surface sampled by photograph cannot be guaranteed to be representative of all the material in the tray.

In the study by Lu and Latham [10], 72 library photographs were produced for 72 different sieve size distributions and a selection was used to calibrate a photo-scanline method. The spacing distribution of particle edge to scanline intersections obtained from superimposing scanlines on the library of photographs were used to generate formulae that relate the $s_c(p)$, $n(p)$ values of the spacing distribution to the s_c, n values of the expected sieve size distribution. Here, $s_c(p)$ and $n(p)$ are simply the best-fit Rosin–Rammler coefficients for the particle segment length distribution obtained from the composite scanline for each photograph of known sieve size distribution. The formulae obtained from the manual scanline analysis using simple linear

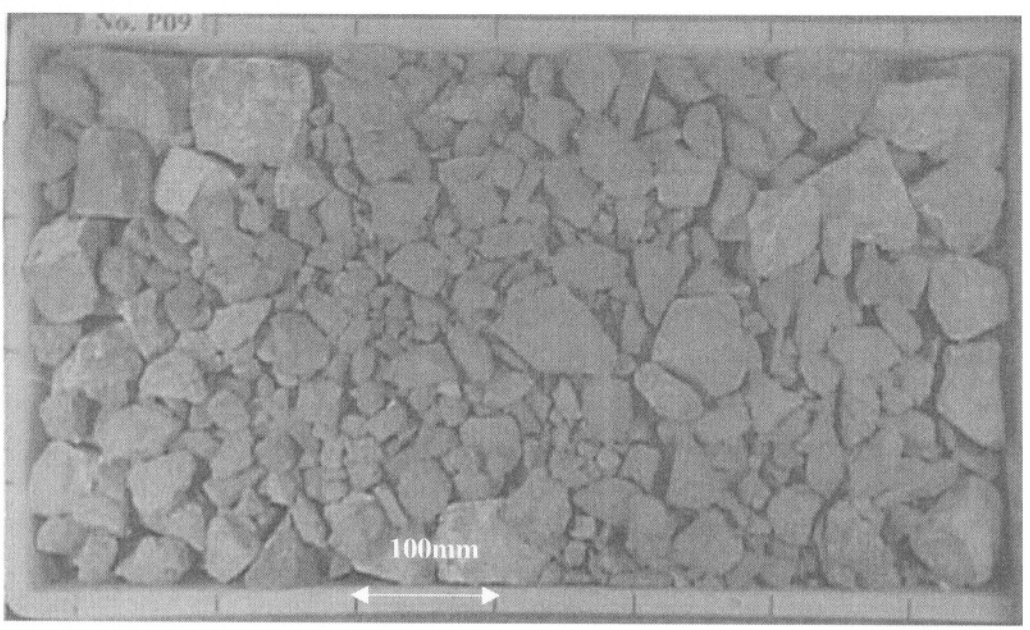

Fig. 1a. P09. Sieve analysis: $S_c = 40$ mm, $n = 1.75$. Note 100 mm scale divisions marked on tray.

regression are given in Equations (4) and (5).

$$S_c = 1.119 S_c(p) \tag{4}$$

$$n = 1.096 n(p) - 0.175 \tag{5}$$

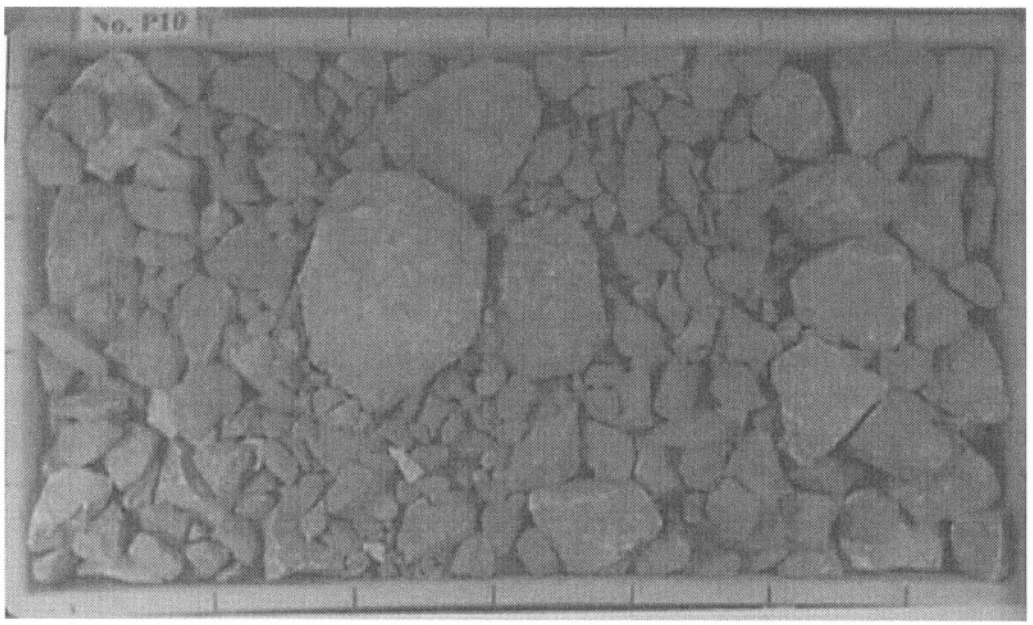

Fig. 1b. P10, Sieve analysis: $S_c = 60$ mm, $n = 1.35$.

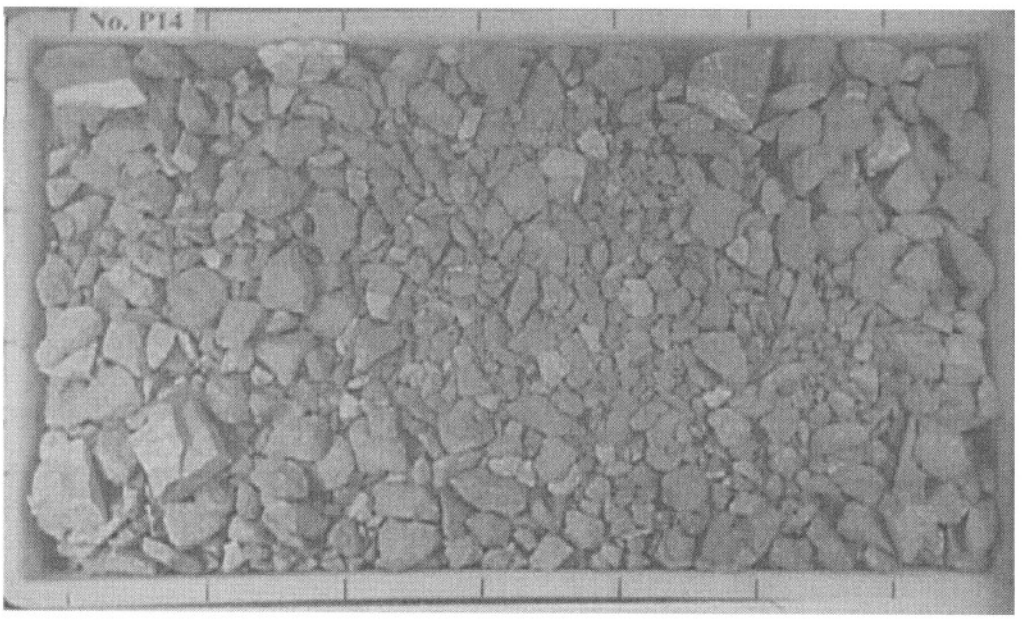

Fig. 1c. P14, Sieve analysis: $S_c = 20$ mm, $n = 1.75$.

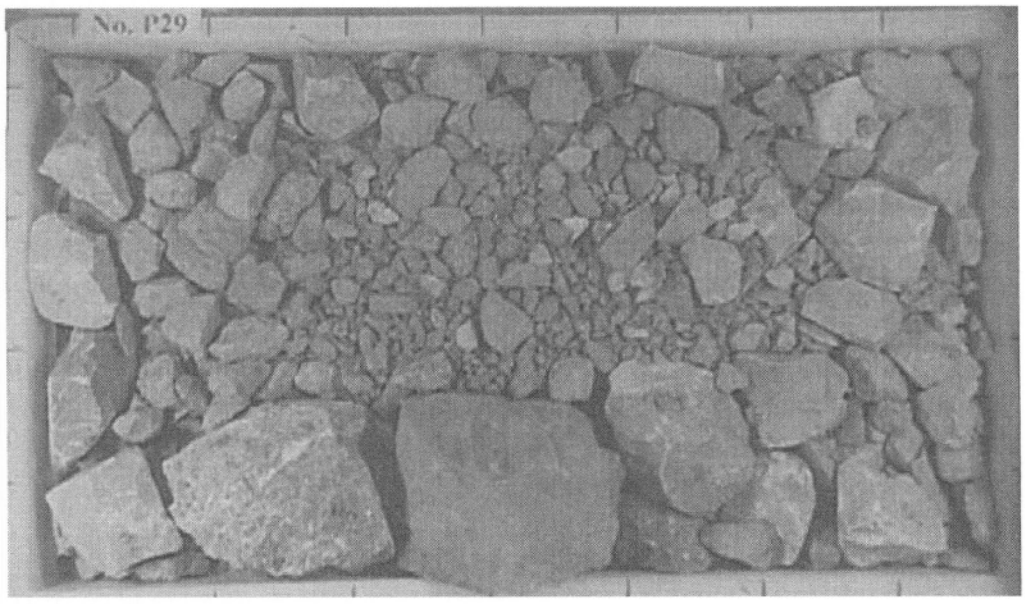

Fig. 1d. P29, Sieve analysis: $S_c = 65$ mm, $n = 0.9$.

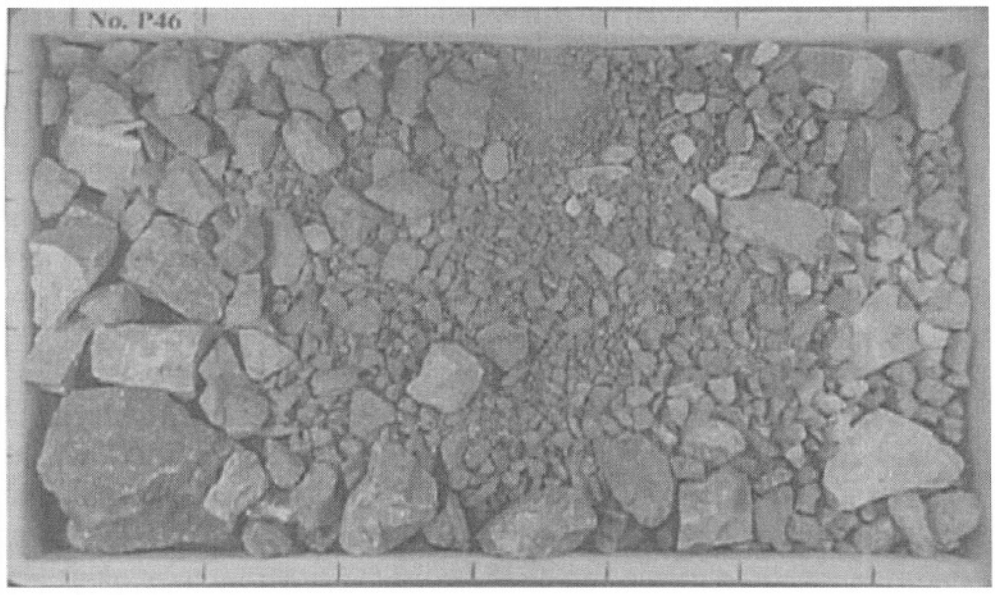

Fig. 1e. P46, Sieve analysis: $S_c = 30$ mm, $n = 0.9$.

The r-squared correlation coefficients for the regressed sieve size prediction of s_c, and n were 0.95 and 0.97 respectively, which is somewhat higher than the r-squared values found for the four automated systems as discussed later in Table 2. Another similar pair of equations were calibrated to give S_{100} and m coefficients to allow use of the photo-scanline method with the Schuhmann model.

1.5. Photo Images

Ten A4-size black and white prints from the photo library were selected to represent a reasonable range of S_c and n-values. These were presented for analysis at the Fragblast workshop and digitised by equipment demonstrated by Tom Palangio (of the WipFrag group). For the purpose of the analyses, the supplied photograph images were captured using a Mavica digital camera. Thus, the image has been captured twice, first by analogue photography and then by a digital system. These were saved as ten JPEG files ranging from 46 to 64 kbytes in size at a resolution of 640×480 pixels (at 118 pixels per cm). These image files were electronically transferred to all four groups for further analysis, thus ensuring identical image input resolution. Examples of the images are given in Figure 1 and the complete set is shown in Figure A1.

2. COMMENTS FROM SYSTEM INVENTORS

2.1. WipFrag

The emphasis of WipFrag analysis is more on precision than accuracy [11], catering more toward process control rather than specification oriented applications. As such, when accuracy (matching sieving) is required, empirical calibration must be employed. In addition, as with other systems, WipFrag requires multiple images for a 3D size analysis of a given assemblage of rock. In this comparison exercise, re-mixing and re-imaging of the sample would have proved useful. Thus, the results of this WipFrag analysis were generally good, but some results were not as good. This may be attributed to the lack of available calibration models. A standard calibration procedure (i.e., a WipFrag standard fines correction) was therefore applied for this study.

For the purpose of these analyses, the images were imported to WipFrag and manual editing was limited to a few minutes per image to improve the fidelity of the block outlines. Of the seven samples with Rosin–Rammler n-values of 0.9 to 1.75 (where calibration is not as much of an issue), one of the results was extremely accurate (P09), three were very close (P01, P10, P29) and three had n-values that were very close but S_c values that were somewhat too coarse (P14, P32, P46).

Of the three remaining samples (P49, P59, P67), those most dependent on calibration, the n-values reported by WipFrag were high, although the S_c values were very close. This is simply because there was no reliable calibration model to base the analysis on.

2.2. Split

The analysis was conducted by a skilled software operator. The images were cropped so that the walls of the container weren't visible and confusing to the delineation

algorithm. A few minutes (< 5) per image was spent correcting the most obvious errors and filling fines. Delineation parameters were set at the standard ones in use at the time ("likely to have been noise 7, shed size 1.5, gradient 0.14 and even lighting"). Fines correction factors of 10% for P01 and P10, and 30% for the remaining photos, were introduced at settings that were subjectively judged to be the optimum ones for this set of photos.

Overall, the results presented in the paper are a good representation of the Split processing algorithms at the time the study was conducted (1999). A certain amount of error is to be expected in single image analysis. For instance, Split overpredicts the S_c in photograph P67. Looking closely at the image, the particles in the photograph do in fact appear large for a Characteristic Size of 35 mm. This is thought to be due to the difference between what appears on the surface for this dumped sample of wide grading compared with the actual size distribution, and this effect is independent of the processing algorithms being used. Further mixing and imaging might reduce these kinds of errors.

2.3. FragScan

The previous and somewhat similar exercise performed by NORANDA [6] showed that FragScan was likely to underestimate some fragments of smaller size. At about that time, internal tests (i.e., ones directed by FragScan inventors) on different versions of the system showed what was summarised as "a really good agreement between true and measured fragmentation." These tests were performed on crushed aggregates and boulders for which the true fragmentation was known but where all samples had a steep uniformity index, owing to a lack of confidence, at that time, in building small-scaled representative samples with low uniformity. Thus, for this and other reasons, there was a reluctance to revise the FragScan program as a result of Liu and Tran's work. However, significant improvements in the system are expected to follow from the comparison study reported here. The present blind test, by contrast with the earlier comparison study, should be considered as objective and achieved in excellent conditions (quality of image lighting and contrast, close to no overlapping of fragments).

For the analysis, processing time for each image was about seven seconds on a Pentium II 305 MHz machine for eight size-classes. No interactive manual intervention was used. However, using FragScan on site, it is normal to adjust a "thresholding" function during the system calibration procedure. Any lowest size limit for the resolution limit can be set and for this study, it was set at 5 mm. Any set-up for number of classes and increment from one class to the next may be chosen.

Commenting more specifically on the results, the FragScan results sensitively follow the actual trends for the sieve variations of S_c and n, as shown by the statistical

analysis, but present an excessive bias for n. The system is behaving as a stiff sensor to variations. Owing to the absence of a fines correction, smaller fragments are neither inferred, nor seen, and thus not taken into account, pushing the curve to the coarser sizes and making it steeper. From further looking at the results, it is possible to point out some imperfections in the FragScan algorithms and these have subsequently been adjusted by "changing the structuring element for the opening process." These imperfections were:

(i) attribution error: fragments significantly delineated into the wrong size-class;
(ii) contamination: a loss of surface of larger fragments which are placed into the central classes.

"Fines correction" is still a subject of discussion amongst FragScan inventors. It is fundamentally not possible to measure with an image-based process something that cannot be seen. Two possibilities that have been adopted variously by other system inventors to tackle this are:

(i) an intelligent extrapolation;
(ii) an empirical correction.

The FragScan inventors hope to draw upon several sources of research in its quest for a 'fines correction' strategy. In a recent study aimed to predict fragmentation from blasting and rock-mass parameters, it appeared that from a consideration of fragmentation mechanisms, the fragmentation of blasted rock was likely to be of a double-component nature [12] which could then be modelled by the sum of 2 log-normal distributions. Such a model might help to extrapolate the population of fines and obtain significant percentages of finer fragments.

Following previous work on the probability of a fragment appearing on the visible surface of a sample (e.g., [13]), it has been noticed that the ratio of visible and identifiable particles versus those present in the sample quickly diverges from 1 as the size of the particle decreases. As an example, for an image of a sample of 10–80 mm fragments with a scale of 0.7 mm/pixel, 15% of particles of size-class 14–20 were not seen, and 45% for the 10–14 mm were not seen. The effect of gravitational segregation (that tends to occur in the preparation of benchmarking samples and in real blastpiles where small material will tend to fall away from top surface views) in this example is thought to be small and is not the reason for the surface sampling bias.

Application of a "correction-vector," a value for each size-class to be multiplied by the raw number of fragments obtained with the image-process, is under investigation. Defining these values will obviously be an empirical process. Combining and fine-tuning these developments will require further experimental work. Further use of the 72-sample photo-library [10] exploited in this paper, could also play an important part in future refinements to FragScan.

2.4. PowerSieve

PowerSieve® was not designed to deliver a 3D distribution from the 2D surface distribution. No image-based system can measure the actual bulk fragmentation distribution, only extrapolate from the surface fragmentation using assumptions about the relationship between the surface expression (including biases relating to the probability of appearance at the surface) and the bulk content – an injected assumption that adds to the uncertainty in the measured distribution. As such, PowerSieve® was designed to assess changes in the surface expression between different distributions of similar rock type and shape [14] with the assumption that the surface biases remain constant between distributions that are sampled in the same way.

The results obtained for PowerSieve® show that assessment of the change in distributions between samples has been quite good. There was excellent agreement both in the trend and magnitude of the assessment of the characteristic size for the first five distributions shown in Figure 2, while the trend (in a broad sense) was well reproduced in the distributions with relatively constant (large) characteristic sizes. The assessment of the uniformity index for each distribution shown in Figure 3 was also remarkably successful.

Overall, PowerSieve® has followed the behaviour of the other systems across the ten distributions. While it has tended to underestimate the characteristic size for the coarse distributions, it has performed very well on the finer distributions. This is

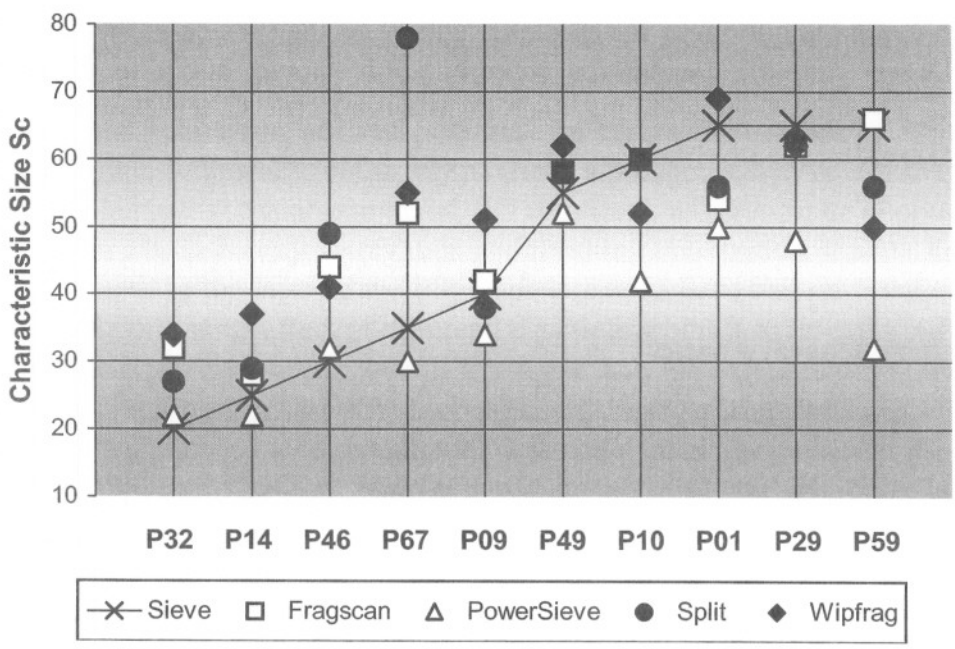

Fig. 2. Characteristic size S_c, from direct sieve results compared with predictions from four systems.

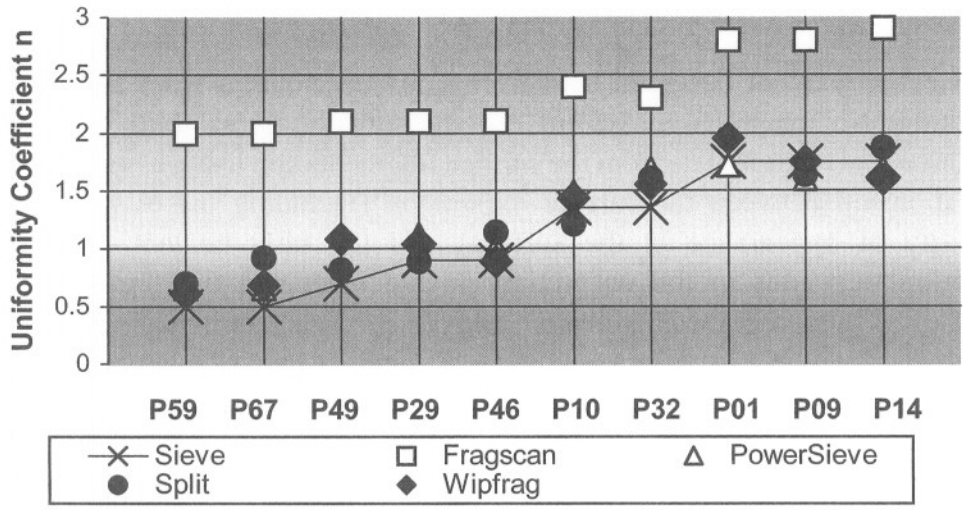

Fig. 3. Uniformity coefficient n, from direct sieve results compared with predictions from four systems.

believed to be because the finer distributions (P32, P14, P46, P67, P09) provided a much better sample of the tails of the distribution with the container not having a marked influence on the spread of the particles across the surface. With the coarse distributions the large particles represent significant concentrations of mass that were essentially unable to flow in the container like the finer particles which spread out to cover the rest of the area of the container. Thus, an overrepresentation of the area of finer particles relative to the area projected by the coarse particles may have occurred. Given a big enough container of sufficient depth such that the largest particle could not both touch the bottom of the container and be on the surface of the pile (hence a much larger sample), the surface representation should begin to approach the sampling situation seen with the finer distributions, for which PowerSieve® did extremely well.

3. RESULTS

3.1. Sample Characteristics

It may be argued that the particle views exposed on the surfaces of the experimentally produced piles, as shown in the photos, are not a representative sample of the particles that make up the whole sieve-analysed sample in the tray. This problem of benchmarking computer systems and interpreting results from sample photographs of surfaces of blastpiles is well known, was commented upon by system inventors (Section 2), has been widely discussed (e.g., [15]) and is further commented on below.

For a photograph of a 'surface view' to be representative of a homogeneous particulate mass with any size distribution, it is necessary to assume many things but

in particular, that the surface presented in the photographs is equivalent to the surface that would be created if

(i) there was no influence of size and shape segregation,
(ii) the sample mass was sufficient for the least uniform gradations to be well represented at the coarse end,
(iii) on examining a theoretical arbitrary (e.g., horizontal) plane through the bulk volume of the sample, all particles above those which are represented within that plane are removed and the in-plane particles are 'frozen' in their positions.

Unfortunately, in practice, even for controlled experiments that are used to calibrate systems using sieved piles, it is difficult, if not virtually impossible to create samples for photography where the above assumptions apply to the observed surfaces. The assumptions break down to a progressively greater degree for less uniform gradations not only in real situations where materials are on the move and thus segregate under gravity, but also in artificial piles designed for calibrating and benchmarking. For non-uniform gradations, calibration piles created by Maerz and Zhou [5] (1999) appear well controlled and probably go a little further to uphold the above assumptions than those in this study.

To create an absolute prediction of the unseen bulk sieve size distribution from the sample of the surface view requires a method to account for the different biases that are likely to be introduced, for example, when these assumptions are broken to a greater or lesser degree. Consider the experimental preparation of artificial blastpiles in the trays described here, when the piles with low S_c and high n-values are dumped in the tray, the above assumptions hold well and the surface view represents the bulk sample with little or no bias. When S_c is large and n-values are low, some segregation is inevitable and the effect of the shallowness of the tray may cause spurious representation of larger pieces and a spreading out with possible over-representation of fines. It may also be argued that the shallowness of the tray has helped prevent gravity segregation of the fines to levels beneath the coarse material. For smaller S_c with moderate n-values there may have been a little gravity segregation and resulting obscuration of fines, however, the shallow depth to the base of the tray appears not to have had an influence. It is therefore likely that some effect of differential sampling bias is to be expected even in the controlled experiments described in this paper but, the extent is not known. The original intention was that this effect would be small when compared with the very significant differences in sieve size distributions created for the experiments.

An evaluation of the four image analysis systems can be based on two considerations, (i) how accurately they assess the mass distributions from an assessment of the surface distribution and (ii) how well they assess the relative differences in the distributions. Although the ten samples presented vary widely in distribution characteristics, a differential sample bias between the distributions (brought about by sample dumping and containment that allows only the finer

particles to flow in the dumping process) may have affected the relative assessment by all systems. Interestingly, the only trend that is consistent to all systems is the underestimate of the proportion of fine material, whereas coarse material is both over- and underestimated for different systems considering the same photographs, (see Fig. 7). The assessment of how well the different systems cope with different distributions has therefore been obscured by the different surface biases associated with each sample but the effect of this bias is thought to be only slight.

The method invariably recommended for industrial application of the various systems to account for the differential sampling bias is to calibrate numerous on-site results against sieve results derived through other reliable means – simple enough for conveyed materials but usually problematic for blast fragmentation assessment. For blast fragmentation assessment, Split and WipFrag offer standard corrections aimed at addressing the tendency for fines to be underestimated from surface views. These two systems therefore directly address the problem, common to many users, of accounting for the most pronounced effects of differential sampling bias, namely the under-representation and poor resolution of fine particles in surface views. However, these two systems offering standard corrections cannot be expected to account for the unpredictable effects of gravity segregation.

3.2. General Results

General results of the different systems can be appreciated by plotting sieving results together with those predicted by the four systems. As the sieve analysis was made to conform to specific pairs of Rosin–Rammler coefficients, the various systems' results have been summarised using these coefficients. The coefficients were obtained by linearised least squares regression of cumulative % passing values that include data points from the lowest size range accommodated by the system settings up to the first 100% passing size examined by the system concerned. The lowest percentage passing size considered by FragScan and PowerSieve® was 10 mm, whereas for Split and WipFrag, it was nearly always 5 mm before fines correction and down to 1 mm after applying the correction. The results are given in Table 1.

The characteristic particle size S_c, in the photo series ranges from 20 to 65 mm. Results in Figure 2 indicate that PowerSieve® gives generally lower S_c values than the other systems and notably good predictions for the case of small S_c photos, (including the wide gradation photo P67), but notably poor predictions of the larger S_c photos. For all the other systems, the general trend is to overpredict S_c for smaller S_c photos and to under-predict S_c for larger S_c photos. It is perhaps reasonable to expect this effect, since it may be assumed that the default setting of most systems will have been configured for an anticipated mean particle size (for the full set of 10 photographs). On cursory inspection of the photos, this would appear to be about 30 to 40 mm. Photographs with mean sizes well below and well above the assumed means for the

Table 1. Rosin–Rammler coefficients determined by image analysis of ten photographs using four different systems.

Photo	Sieve		FragScan		PowerSieve®		Split fines corrected		WipFrag fines corrected	
	n	S_c	n	S_c	n	S_c	n	S_c	n	S_c
P32	1.35	20	2.3	32	1.69	22	1.61	27	1.55	34
P14	1.75	25	2.9	28	1.69	22	1.87	29	1.59	37
P46	0.9	30	2.1	44	1.02	32	1.14	49	0.89	41
P67	0.5	35	2	52	0.66	30	0.92	78	0.68	55
P09	1.75	40	2.8	42	1.6	34	1.63	38	1.75	51
P49	0.7	55	2.1	58	1.11	52	0.82	58	1.08	62
P10	1.35	60	2.4	60	1.49	42	1.21	60	1.43	52
P01	1.75	65	2.8	54	1.72	50	1.95	56	1.95	69
P29	0.9	65	2.1	62	1.12	48	0.89	63	1.05	62
P59	0.5	65	2	66	0.66	32	0.7	56	0.61	50

photo series as a whole, are likely to generate some bias (which may be minimal) simply because the most accurate range of bin widths will be under-used.

The uniformity coefficient n, ranges from 0.5 to 1.75 in the photo series. There can be little doubt that the surface views sampled by the photos with higher uniformity indices (higher n-values) are close to being representative of the sieved material. Some doubt may exist for photos with lower uniformity indices. Figure 3 shows clearly how FragScan consistently predicts a more uniform range of sizes than is predicted by other systems, and by an amount equivalent to an increase in n, over and above the sieve value, of between 1 and 1.5. The photos with the most uniform sizes, (ones with n=1.75) in increasing order of S_c are P14, P09 and P01. For each of these photos, n-values are closely predicted by the three systems, PowerSieve®, Split and WipFrag. For photos with n below 0.9, these three systems tend to predict only slightly higher uniformities than are present according to the sieve values. Thus, it is possible that the amount of fine material masked behind larger pieces in these photos is reasonably typical of particulate surfaces and conditions for which the standard calibrations employed in this study would apply.

The observed level of agreement and bivariate statistics for sets of sieve and system-predicted results for the ten photos are also shown in Figures 4 and 5 and given in Table 2.

It may be argued that it is also reasonable to look at the same overall statistical analysis of results when the photographs that yield outlier results e.g., P67 and P59 are excluded. The rationale for this is as follows. The large areas of material of < 2 mm in P67 and P59 appear to have been treated in various different ways. For example, by automated settings that combine these fines into a single coarse particle, by automated settings that attribute these fines to fine material below resolution, and by manual edit

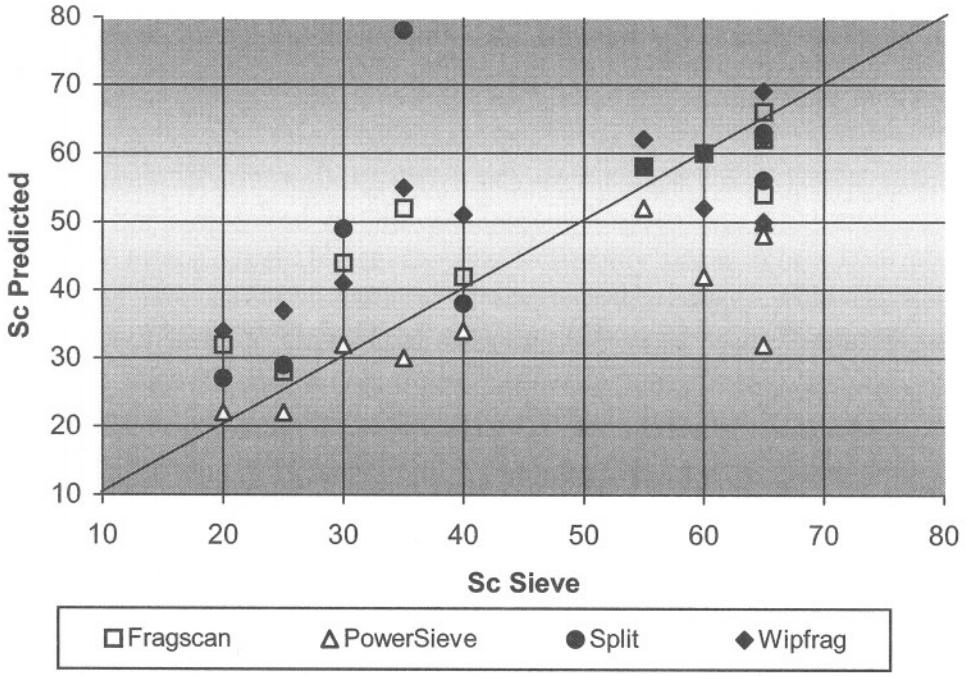

Fig. 4. Scatter plot of S_c values as predicted versus S_c values from sieve analysis. Note. in-filled square is for coincident FragScan and Split results.

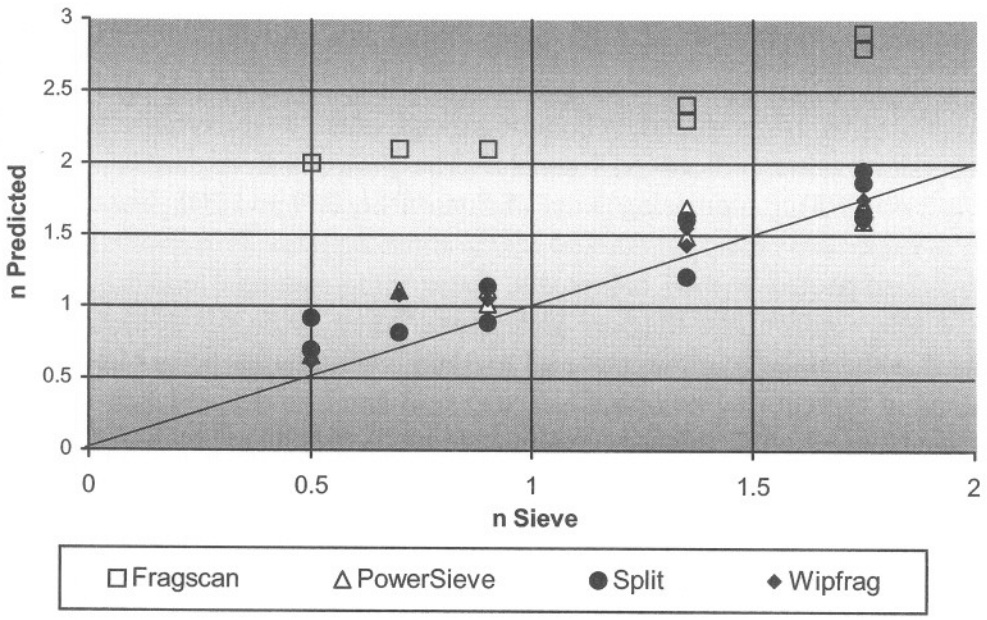

Fig. 5. Scatter plot of n values as predicted versus n-values from sieve analysis.

removal prior to the automated analysis as these fines are presumed to be the base area of the tray containing no particles. Removal of the P67 photo from the group analysis has a large influence on the apparent performance of the Split system.

Table 2. Statistic indicators of the agreement between Rosin–Rammler coefficients determined by image analysis systems and those from direct sieving analysis.

Statistic	FragScan		PowerSieve®		Split		WipFrag	
	n	S_c	n	S_c	n	S_c	n	S_c
R^2	0.956	0.901	0.949	0.825	0.939	0.592	0.959	0.815
Std. error	0.111	5.91	0.140	6.42	0.166	13.65	0.139	7.00
$SS = \sum(x_p - x_s)^2$	14.87	782	0.44	2014	0.44	2454	0.32	1345
$SS^* = \sum(x_p - x_s)^2$	10.37	492	0.39	900	0.23	524	0.28	720

Note. The R^2 correlation coefficient is given by covariance divided by the product of the standard deviations and assesses the correlation, not the absolute prediction. Standard error (Std. Error) is given for a linear regression model that allows an intercept. Forcing the regression through the origin may be considered more meaningful. The sum of the squares (SS) given is that for the differences between the system prediction value and the sieve value. SS^* is that based on eight photos that exclude P59 and P67 (see text).

In summary, all systems show a high R^2 for n. The FragScan system gives the most correlated predictions for S_c and n as shown by high R^2 and low standard errors for the regression. The FragScan SS values for S_c are also the lowest, suggesting FragScan is a good predictor of the S_c sieve value. However, as is also apparent from Figures 3 and 5, SS values for n indicate FragScan is a poor predictor of the complete sieve size distribution. This suggests that simple further refinements to the FragScan system might lead to an improved prediction of sieve results for the whole grading. WipFrag and PowerSieve® are generally the next best predictors of the sieve S_c and n-values.

With the two low uniformity outlier photos excluded, the overall performance of Split is much better, showing lower SS^*-values than WipFrag. Split would appear nearly as good as FragScan for predicting the sieve S_c-values.

3.3. Detailed Results

To look at the results in more detail, the histograms and cumulative curves for each photo produced by each system have been examined. In order to present such curves and histograms, it was considered necessary to obtain the histogram analysis using the same bin size intervals that were used in the original sieve analysis. PowerSieve® was not able to provide such a reanalysis at these desired sizes. The PowerSieve® histogram results were therefore converted by linear interpolation from the 10–20, 20–30, 30–40 mm etc. bins to 10–14, 14–20, 20–31.5 mm etc. bins. No attempt has been made to interpolate PowerSieve® values into intervals below 10 mm and the PowerSieve® histogram entries are left blank for these small size intervals. The three remaining systems were able to generate histogram data from the photos using the same size intervals as in the original sieve analysis. Note, the Split operators

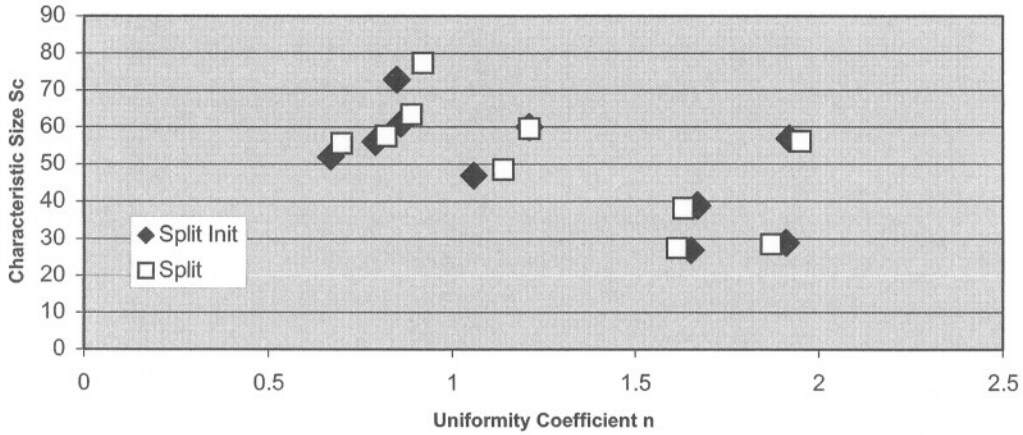

Fig. 6. Plot showing small changes in the Split results from the results originally reported at the Fragblast 6 workshop (Split Init) and those reported in this paper.

resubmitted a set of results using their original grain delineation files but at the correct scale unit of 100 mm, which had erroneously been given as 50 mm in their first analysis. Some small changes from their original Fragblast 6 workshop results were detected in the resulting Rosin–Rammler coefficients, as shown in Figure 6. These changes do not compromise the integrity of the blind comparison, as suggested by Figure 6, which shows there has been no reworking to improve predictions.

A selection of histogram results corresponding to the photos in Figure 1 is shown in Figure 7. The results displayed in histogram form show the mass fraction in each size interval. This enables a direct consideration of the size intervals that give a good agreement with the sieve analysis, for each system. To bring out more clearly the effect of the fines corrections, results are presented with and without the fines corrections for the Split and WipFrag systems. Figure 8 provides further means for comparing histogram results with those from the sieve analysis. (However, note that PowerSieve® results are spurious for intervals < 10 mm in this figure owing to the zero entry shown in Fig. 7). The cumulative (PSD) curves are given in Figure 9. It is perhaps worth pointing out just how clearly the format in Figure 8 shows the very good performance of the fines corrected SPLIT system across all size ranges in P09, P10 and P14, as expressed by the predicted PSD curves practically sitting on the sieve curves in Figure 9. Note also that for many applications, the visually assessed difference between predicted and known sieve curves is best viewed with a logarithmic scale for the size axis.

3.4. Discussion of Individual Photos

3.4.1. P09

In P09, the fines corrected SplitC results follow remarkably close to the sieve analysis throughout while WipFragC is also close but over predicts the percentage in the

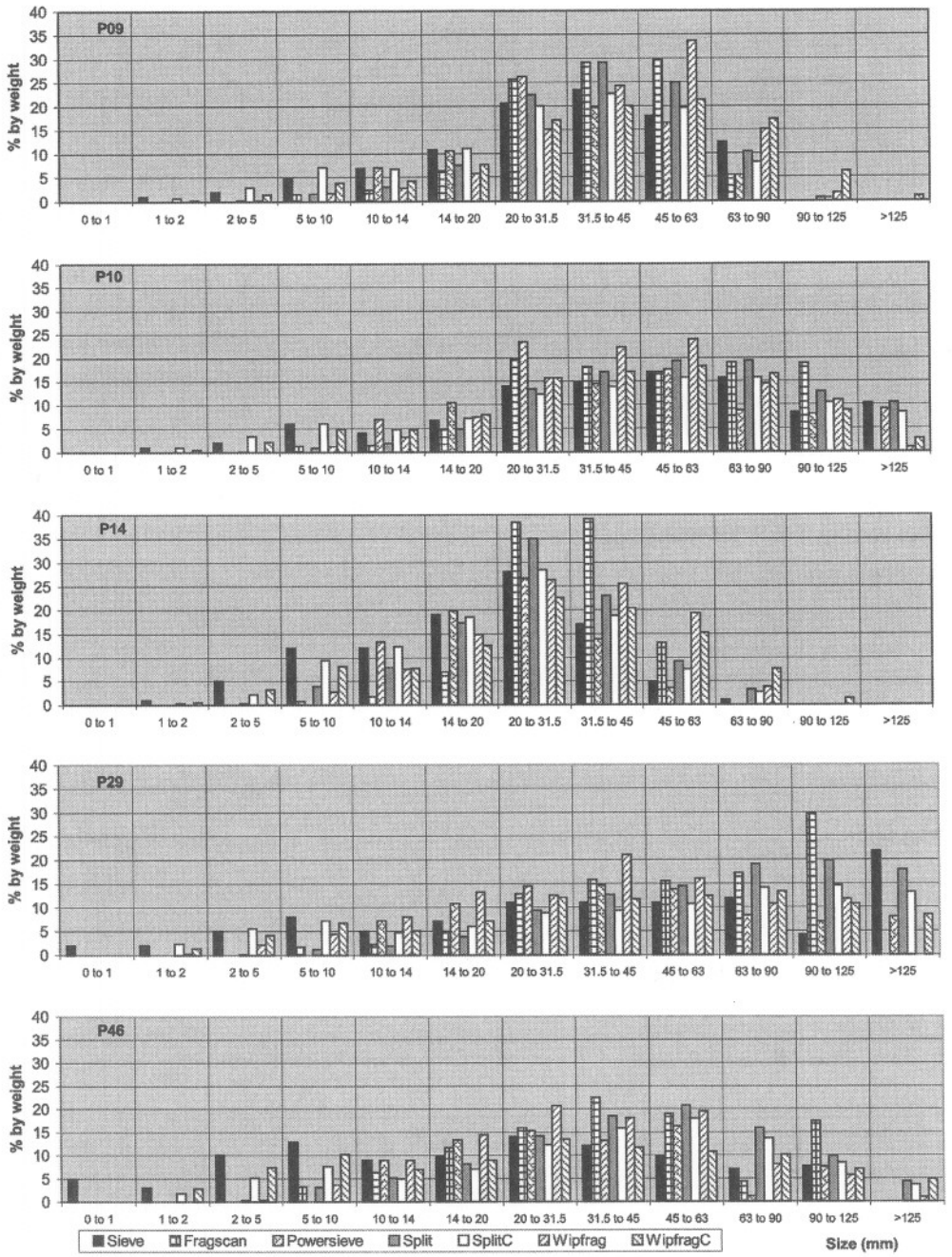

Fig. 7. Selected size analysis results presented in histogram form.

coarser size intervals. PowerSieve® is remarkably close to the sieve analysis in all size intervals below 63 mm. Below 20 mm, FragScan steadily under-predicts the percentage below 20 mm and over-predicts above 20 mm. Both Wipfrag, and to a greater extent Split, without the fines corrections, are similar to the FragScan results.

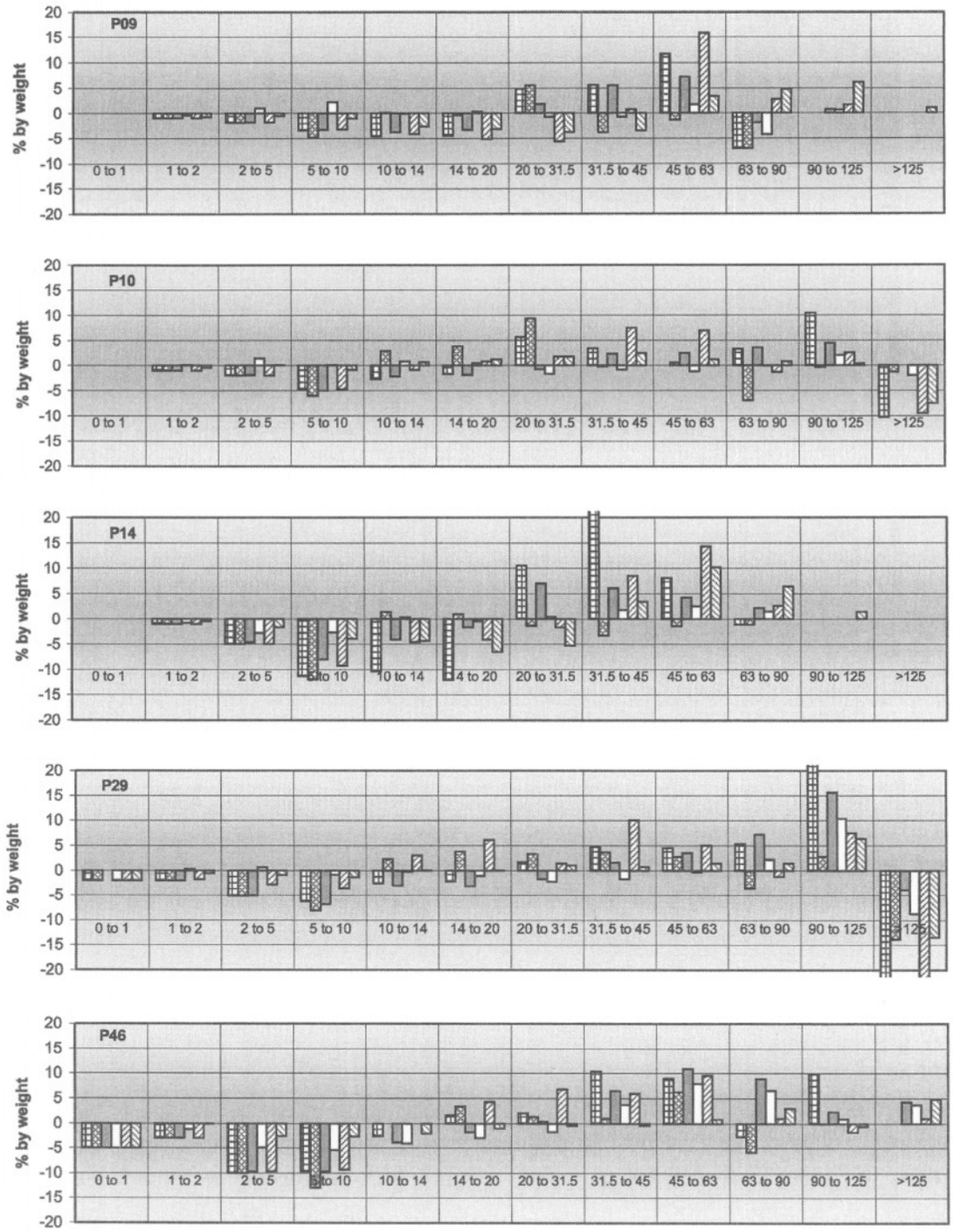

Fig. 8. System prediction minus sieve analysis for the percentage-by-weight within each size interval.

3.4.2. P10

In P10, a slightly coarser and wider sample grading, WipfragC and SplitC both give excellent predictions. PowerSieve® consistently over-predicts the 10 to 30 mm

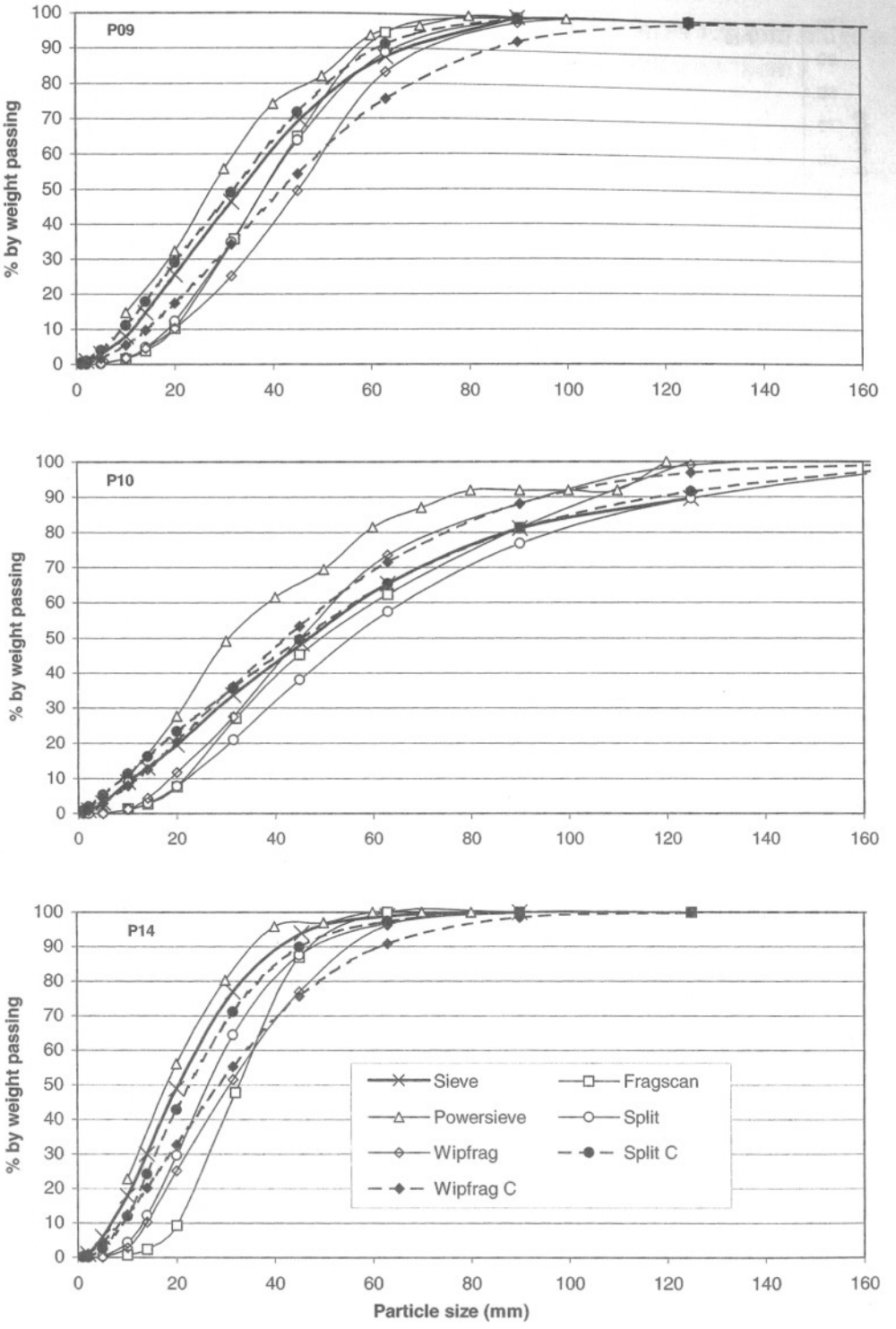

Fig. 9. Predicted and sieve analysis PSD curves for selected photos, together with sieve analysis PSD curves for all ten photos.

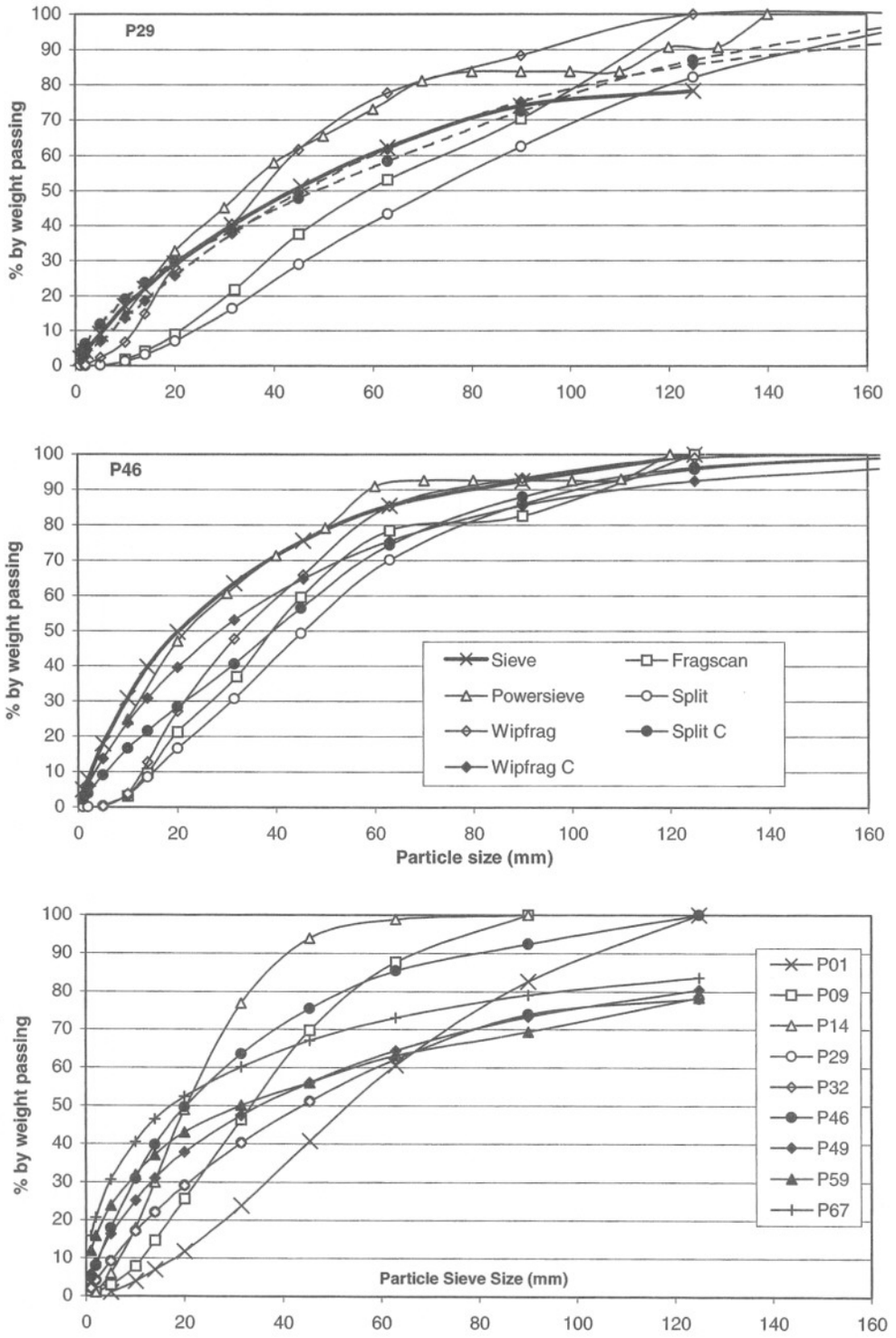

Fig. 9. (*continued*).

percentages. FragScan overpredicts the percentages in the 90 to 125 mm range a little more than the other uncorrected systems but is broadly similar to them.

3.4.3. P14

This is a good test for a uniform size distribution. Wipfrag and WipfragC appear to overestimate the percentage in the ranges 30 to 90 mm whereas for some reason, the Split and SplitC overprediction is less marked. PowerSieve® has remarkable success with this image. FragScan attributes far too much to the 30 to 63 mm ranges but correctly shows no material above 63 mm.

3.4.4. P29

Curiously, the uncorrected versions of Split and WipFrag perform best in different parts of the size spectrum. This widely graded coarse sample illustrates the effectiveness of both the fines corrected WipfragC and SplitC (especially if a single coarsest interval of >90 mm is introduced, which can be justified in this case because of the two blocks of about 125 mm in the photo). PowerSieve® consistently over-predicts the percentages in all intervals from 10 to 63 mm. FragScan consistently under-predicts for all small size intervals up 20 mm and thereafter overpredicts.

3.4.5. P46

P46 is a wide grading of smaller sizes, where the PowerSieve® and WipfragC predictions are remarkable throughout all size intervals. FragScan greatly overpredicts the percentage of material in the 30 to 63 mm intervals, as does the uncorrected and corrected Split.

4. CONCLUDING REMARKS

It would be unwise to single out particular systems in the conclusions as all four systems have particular merits not to be dismissed. The user of automated size analysis systems will benefit from studying these results and the warnings implied by the extent of errors and the variability of any one system's performance in assessing ten widely differing images. Depending on the objective, be it tracking a shift in S_c during production, accurate determination of either S_{10}, S_{50}, S_c or S_{95}, or, accurate absolute determination of gradings, varying from extremes of large and small S_c as well as narrow and wide gradings, the results presented in this paper will point towards the favoured operating systems. Whereas all systems can track relative shifts in S_c for narrow gradings, accurate logging of the whole sieve curve in a production sample that varies considerably from one subsample to the next is much more challenging. Application-specific calibration is invariably recommended by the system inventors but this may be an unrealistic luxury for many users. The critical test

of future systems, wishing to promote their versatility, will be based on their proven ability to discriminate small absolute changes in distributions, whether wide or narrow. However, factors such as the degree of gravity segregation expected which is likely to be different on conveyed sample surfaces compared with muckpile surfaces should not be neglected.

ACKNOWLEDGEMENTS

John-Paul wishes to apologise for the delays in working up the results since the Fragblast 6 conference. He would like to thank all the co-authors for their perseverance and help in bringing this exercise to a satisfactory conclusion, while maintaining such a spirit of cooperation. The PowerSieve results were produced by Simon Tose of the AEL Fragmentation Bureau Service and these results agree generally but not precisely with those results produced by PowerSieve in the hands of its software developer, Michael Noy.

REFERENCES

1. Franklin, J.A. and Katsabanis, T.: *Proceedings of the Fragblast-5 Workshop on Measurement of Blast Fragmentation, Montreal*. Balkema, Rotterdam, 1996, p. 315.
2. Cunningham, C.V.B.: Ketnote Address: Optical Fragmentation Assessment – A Technical Challenge, In: J.A. Franklin and T. Katsabanis (eds.): *Proceedings of the Fragblast-5 Workshop on Measurement of Blast Fragmentation, Montreal*. Balkema, Rotterdam, 1996, pp. 13–19.
3. Santamarina, J.C., Morley, M., Franklin, J.A. and Wang, D.S.: Development and Testing of a Zooming Technique for Fragmentation Measurement. In: J.A. Franklin, T. Katsabanis (eds.): *Proceedings of the Fragblast-5 Workshop on Measurement of Blast Fragmentation, Montreal*. Balkema, Rotterdam, 1996, pp. 133–140.
4. Kemeny, J., Girdner, K., Bobo, T. and Norton, B.: Improvements for Fragmentation Measurement by Digital Imaging: Accurate Estimation of Fines. In: *Proceedings of the 6th International Symposium for Rock Fragmentation by Blasting*. South African Institute of Mining and Metallurgy, Johannesburg, 1999, pp. 103–110.
5. Maerz, N.H. and Zhou, W.: Calibration of Optical Digital Fragmentation Measuring Systems. In: *Proceedings of the 6th International Symposium for Rock Fragmentation by Blasting*. South African Institute of Mining and Metallurgy, Johannesburg, 1999, pp. 125–130.
6. Liu, Q. and Tran, H.: Comparing Systems – Validation of FragScan, WipFrag and Split. In: J.A. Franklin and T. Katsabanis (eds.): *Proceedings of the Fragblast-5 Workshop on Measurement of Blast Fragmentation, Montreal*. Balkema, Rotterdam, 1996, pp. 151–156.
7. Rosin, P. and Rammler, E.: The Laws Governing the Fineness of Powdered Coal. *J. Inst. Fuel* 7 (1933), pp. 29–33.
8. Schuhmann Jr., R.: Energy Input and Size Distribution in Comminution. *Trans. Am. 1st. Min. Metall. Petrol. Engrs.* 217 (1960), pp. 22–25.
9. Tsirel, S.V.: Methods of Granular and Fragmented Material Packing Density Calculation. *Int. J. Rock Mech. Min. Sci.* 34(2) (1997), pp. 263–273.

10. Lu, P. and Latham, J.-P.: Estimation of Blasted Block Size Distribution of a Blastpile Combining Photo–Scanline Technique With Ros–Ram and Schuhmann Models. In: Guo Yugnang and Golosinski Tad S. (eds.): *Proceedings of the '96 International Symposium on Mining Science and Technology, China*. Balkema, Rotterdam, pp. 683–688.
11. Maerz, N.H.: Automated Online Optical Sizing Analysis. In: *SAG 2001 Conference*, Vancouver, Canada, September 30–October 2, 2001.
12. Djordjevic, N.: Two-Component Model of Blast Fragmentation. In: *Proceedings of the 6th International Symposium for Rock Fragmentation by Blasting*. South African Institute of Mining and Metallurgy, Johannesburg, 1999, pp. 213–219.
13. Chavez, R., Cheimanoff, N., and Schleifer, J.: Sampling Problems During Grain Size Distribution Measurement. In: Mohanty, B. (ed.): *Rock Fragmentation by Blasting*. Balkema, Rotterdam, pp. 245–251.
14. Noy, M.: 2D Versus 3D Fragmentation Analysis: Preliminary Findings. In: *Proceedings of the 13th Annual Symposium on Explosives and Blasting Research*, Las Vegas, February 2–7 1997, pp. 181–190.

APPENDIX

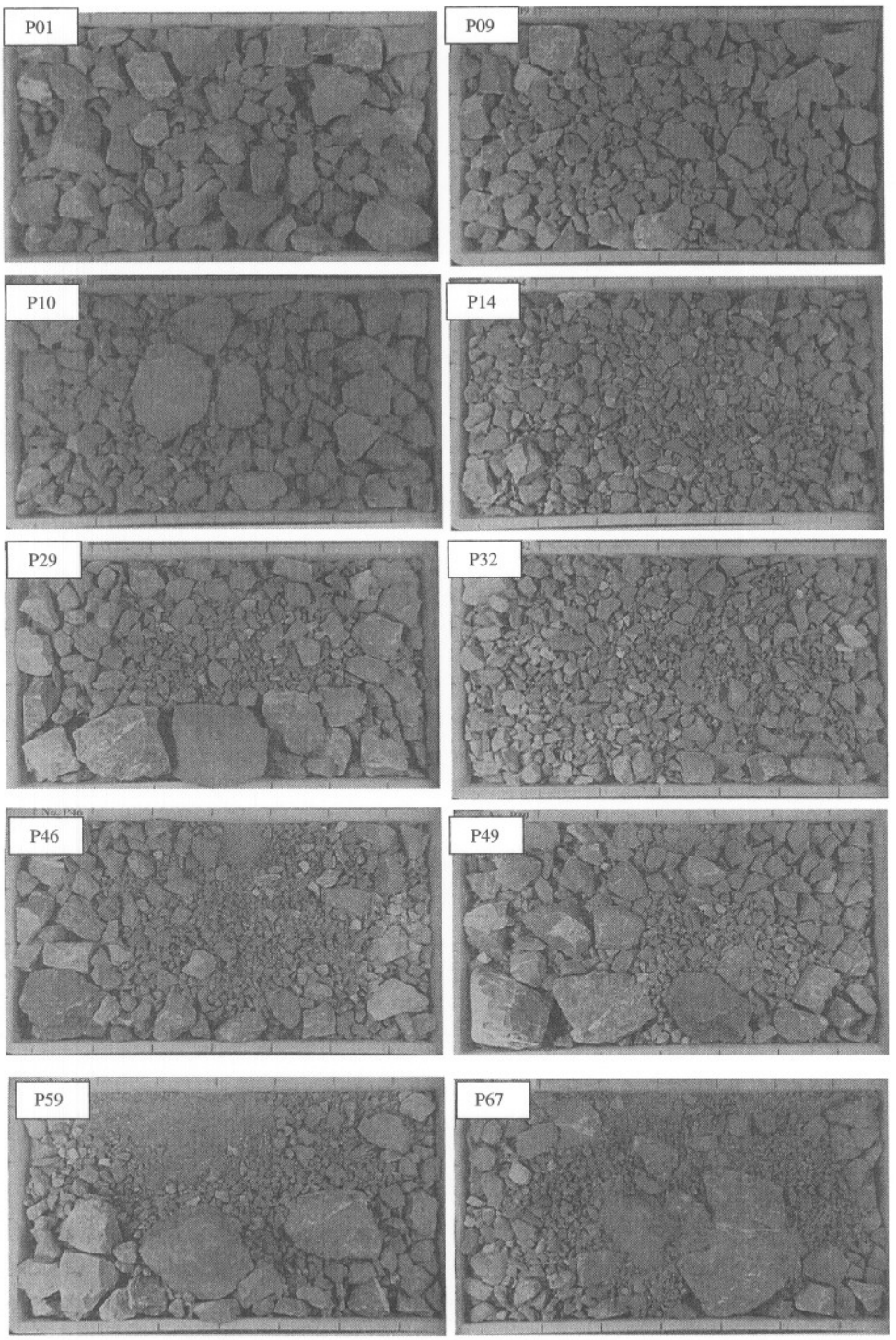

Fig. A1. Ten photos (Scale Divs = 100 mm) selected from the photo library for the comparison study together with their sieve analyses as given in the following table:

Photo	n	S_c	Photo	n	S_c
P01	1.75	65	P09	1.75	40
P10	1.35	60	P14	1.75	25
P29	0.9	65	P32	1.35	20
P46	0.9	30	P49	0.7	55
P59	0.5	65	P67	0.5	35

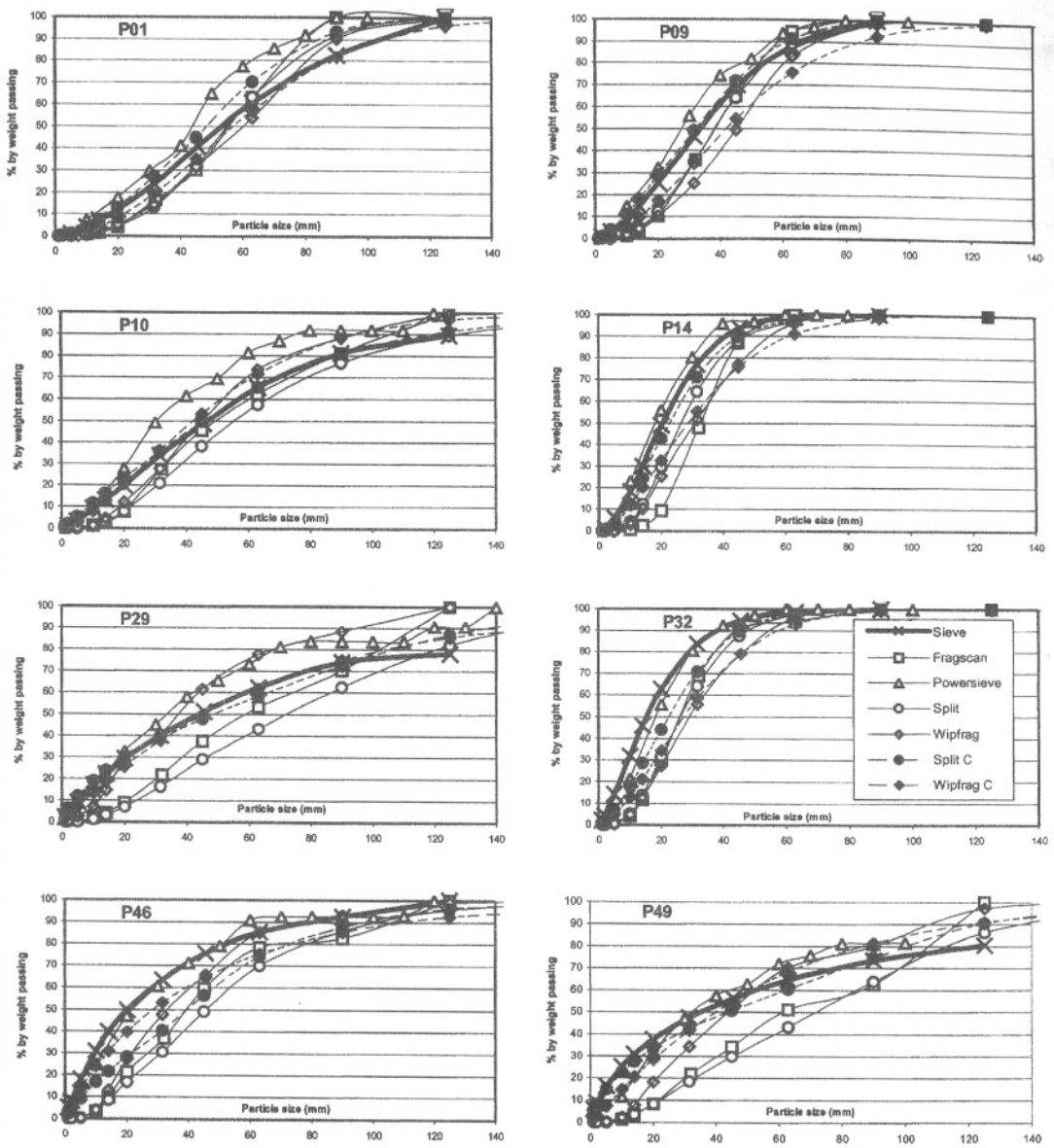

Fig. A2. Complete PSD curve results for all ten photographs analysed.

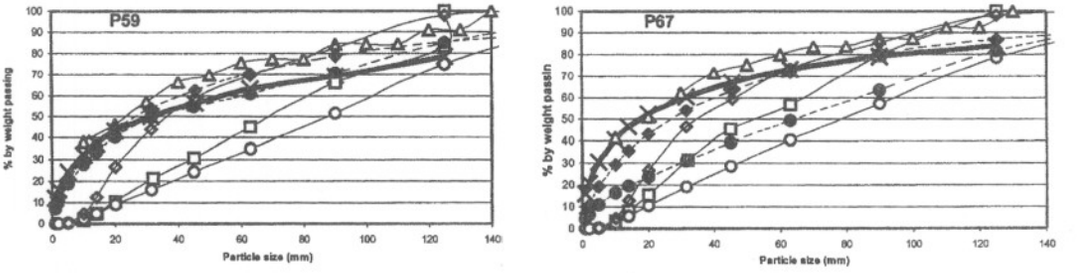

Fig. A2. (*continued*).